

PACIFISTA: Conflict Evaluation and Management in Open RAN

Pietro Brach del Prever, *Student Member, IEEE*, Salvatore D'Oro, *Member, IEEE*,
Leonardo Bonati, *Member, IEEE*, Michele Polese, *Member, IEEE*,
Maria Tsampazi, *Student Member, IEEE*, Heiko Lehmann, Tommaso Melodia, *Fellow, IEEE*



Abstract—The O-RAN ALLIANCE is defining architectures, interfaces, operations, and security requirements for cellular networks based on Open Radio Access Network (RAN) principles. In this context, O-RAN introduced the RAN Intelligent Controllers (RICs) to enable dynamic control of cellular networks via data-driven applications referred to as *rApps* and *xApps*. RICs enable for the first time truly intelligent and self-organizing cellular networks. However, enabling the execution of many Artificial Intelligence (AI) algorithms making autonomous control decisions to fulfill diverse (and possibly conflicting) goals poses unprecedented challenges. For instance, the execution of one *xApp* aiming at maximizing throughput and one aiming at minimizing energy consumption would inevitably result in diametrically opposed resource allocation strategies. Therefore, conflict management becomes a crucial component of any functional intelligent O-RAN system. This article studies the problem of conflict mitigation in O-RAN and proposes PACIFISTA, a framework to detect, characterize, and mitigate conflicts generated by O-RAN applications that control RAN parameters. PACIFISTA leverages a profiling pipeline to tests O-RAN applications in a sandbox environment, and combines hierarchical graphs with statistical models to detect the existence of conflicts and evaluate their severity. Experiments on Colosseum and OpenRAN Gym demonstrate PACIFISTA's ability to predict conflicts and provide valuable information before potentially conflicting *xApps* are deployed in production systems. We use PACIFISTA to demonstrate that users can experience a 16% throughput loss even in the case of *xApps* with similar goals, and that applications with conflicting goals might cause severe instability and result in up to 30% performance degradation. We also show that PACIFISTA can help operators to identify conflicting applications and maintain performance degradation below a tolerable threshold.

Index Terms—Conflict Management, O-RAN, Open RAN, 5G, 6G.

1 INTRODUCTION

The Open Radio Access Network (RAN) paradigm is spearheading the revolution in the telco ecosystem by promoting

P. Brach del Prever, S. D'Oro, L. Bonati, M. Polese, M. Tsampazi, and T. Melodia are with the Institute for the Wireless Internet of Things, Northeastern University, Boston, MA, U.S.A. E-mail: {brachdelprever.p, s.doro, l.bonati, m.polese, tsampazi.m, melodia}@northeastern.edu. Heiko Lehman is with Deutsche Telekom AG, T-Labs, 10781 Berlin, Germany. Email: h-lehmann@telekom.de.

This work was partially supported by Deutsche Telekom, by the U.S. National Science Foundation under grant CNS-1925601, and by OUSD(R&E) through Army Research Laboratory Cooperative Agreement Number W911NF-19-2-0221. The views and conclusions contained in this document are those of the authors and should not be interpreted as representing the official policies, either expressed or implied, of the Army Research Laboratory or the U.S. Government. The U.S. Government is authorized to reproduce and distribute reprints for Government purposes notwithstanding any copyright notation herein.

open, programmable, virtualized, multi-vendor, disaggregated cellular architectures. In this context, the O-RAN ALLIANCE—a consortium of vendors, operators, integrators, and academic partners—is specifying Open RAN architectures, interfaces, operations, and security requirements necessary to realize the Open RAN vision [1].

One of the most disrupting technologies in O-RAN are the RAN Intelligent Controllers (RICs), i.e., the Non-real-time (RT) RIC and the Near-RT RIC. Both host intelligent applications that execute inference tasks (e.g., monitoring, control, forecasting). The former is designed to operate on timescales above 1 s via so-called *rApps*, while the latter hosts *xApps* that perform tasks on timescales between 10 ms and 1 s [2]. This enables dynamic and efficient policy control to reconfigure the RAN and achieve bespoke operator goals while adapting to varying demand and load.

O-RAN paves the way to self-optimizing cellular networks rooted in data-driven policy customization based on real-time RAN performance. In this way, Artificial Intelligence (AI) control enables benefits such as improved efficiency and performance, and reduced energy consumption, among others [3]. However, the co-existence of a multitude of AI-based algorithms taking autonomous decisions to achieve diverse goals (e.g., maximizing performance or minimizing energy consumption) exposes the network to conflicting control policies. An illustrative example of a conflict between two control policies is that of a Throughput Maximization (TM) *xApp*—trying to maximize Downlink (DL) throughput for a Enhanced Mobile Broadband (eMBB) slice—and an Energy Saving (ES) *xApp*—minimizing energy consumption of the RAN. In Fig. 1 (left), we report the control policies (i.e., Physical Resource Blocks (PRBs) allocation for the eMBB slice) computed by the two *xApps* when executing on a real-world O-RAN testbed. We notice how the two *xApps* allocate PRBs differently and according to their individual goals. We also notice that when executing at the same time (i.e., the TM + ES case), the conflicting goals generate unstable control policies that cause an oscillatory behavior. These oscillating control policies are undesirable, because both apps try to achieve their goals—i.e., maximize throughput by giving a lot of resources, or maximize energy efficiency, by assigning very few resources—but none manages to maintain the network configurations that they want to set. Consequently, this behavior hinders performance.

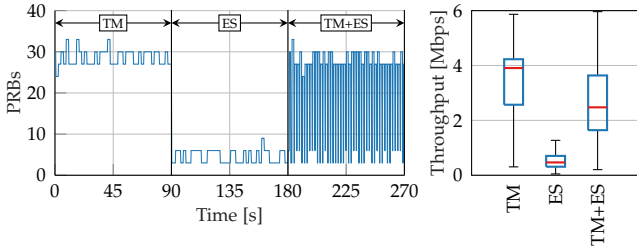


Fig. 1: Impact of conflicts on performance. The xApps for TM and for ES are first run separately and then together. Left: assigned PRBs for eMBB slice. Right: Measured throughput statistics.

Specifically, Fig. 1 (right) shows how xApp TM delivers ≈ 4 Mbps median throughput values, while xApp ES saves energy by maintaining the number of allocated PRBs low (≈ 5 PRBs out of 50). When both TM and ES xApps coexist at the same time, throughput drops by $\approx 50\%$ compared to xApp TM, while resource utilization increases compared to xApp ES, which is a behavior that goes against the intents of both xApps.

In principle, one could avoid the need for conflict management frameworks via conflict avoidance [4]. For instance, one could decide not to deploy xApp ES when xApp TM is active. However, granted this approach might be feasible for small RAN deployments, it would limit the benefits of the RIC, as some conflicting applications might be able to coexist under certain operational conditions. For example, xApp TM would increase resource utilization when there is user demand, but would save resources when there is no demand, which aligns with the goal of xApp ES.

Another naive approach would consider a centralized entity overseeing the entire network. Unfortunately, this approach is impractical as it needs a unified algorithm to control thousands of RAN components and functionalities simultaneously and in real-time, which is unfeasible due to the combinatorial number of actions and network states to be explored. On the other hand, a distributed intelligence approach utilizing multiple xApps and rApps, each controlling specific parts of the network to achieve individual goals, provides a more practical, scalable, and programmable solution. However, how to guarantee that this fabric of AI-based, multi-vendor xApps and rApps makes decisions without generating conflicting control policies—that might result in performance degradation—is still unclear, especially since conflicts can be diverse, observable only at certain timescales, or affecting different network components and Key Performance Measurements (KPMs).

Given the complexity and significance of the issue, conflict management has emerged as a key area of interest within the community, offering a crucial tool for enabling and promoting the adoption of O-RAN. Specifically, the O-RAN ALLIANCE has classified conflicts into direct, indirect and implicit ones (discussed in detail later in the paper). Preliminary efforts in O-RAN conflict management include detecting conflicting control policies in real time [5], [6], performing on-line “deconfliction” [7], coordinating AI-based xApps and rApps via team learning to reduce the occurrence of conflicts [8], [9], as well as orchestrating xApp and rApp selection and deployment to avoid conflicts [4]. While

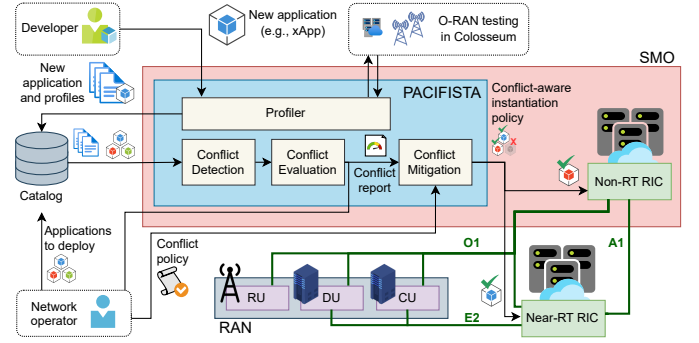


Fig. 2: PACIFISTA architecture and workflow.

these works illustrate concrete efforts to develop solutions that can address and mitigate conflicts in O-RAN, they do not fully examine the nuances of conflict severity and their impact on KPMs. Additionally, they do not consider the possibility that certain conflicts may only become apparent under specific operational conditions (e.g., xApps TM and ES may exhibit a similar behavior when network load is low).

Main contributions. In this paper, we fill this gap by proposing PACIFISTA, a framework to characterize, and evaluate direct, indirect and implicit conflicts in O-RAN. Specifically:

- We design and present PACIFISTA, an empirical and formal framework that draws on statistical information from xApps, rApps and dApps [10] to detect, characterize and mitigate conflicts that might arise between different applications. The architecture of PACIFISTA is illustrated in Fig. 2. PACIFISTA combines the use of a hierarchical graph with the knowledge of the statistical behavior of O-RAN applications to identify relationships between control parameters and KPMs. This enables PACIFISTA to: (i) determine whether two or more applications will generate conflicts; and (ii) quantify the severity of such conflicts.
- We design a profiling pipeline to test O-RAN applications across a set of predefined sandbox tests in different operational conditions. The pipeline generates a mathematical model to infer the existence and severity of conflicts by leveraging the statistical data generated during the profiling phase. We present several statistical indicators and tools that can be used to assess the severity of each conflict and identify affected KPMs and control parameters.
- We demonstrate the capabilities of PACIFISTA via experiments on the Colosseum wireless network emulator and the OpenRAN Gym [11] platform with real xApps, showing that PACIFISTA can predict the occurrence of conflicts and provide accurate information on which KPMs will be affected and to what extent. In this manner, the a-priori knowledge offered by PACIFISTA can be used to evaluate conflicts prior to the deployment of O-RAN applications, thereby facilitating informed deployment decisions regarding which xApps/rApps to deploy to mitigate conflicts.

2 RELATED WORK

Conflict mitigation is a problem that applies in general to distributed systems with multiple agents having access and

control over a set of objects/systems [12]. It is generally tackled using a combination of game theory, access control and coordination mechanisms [7], [13], [14], [15]. In the O-RAN context, the control surface is represented by the wireless portion of the network (e.g., resource management, user mobility, node scaling, among others), whose dynamics are stochastic in nature and hard to predict. This makes conflict management and resolution in O-RAN a substantially different problem than those involved in supply chain, control, and information systems where dynamics are instead more predictable and slowly varying, thus making the approaches mentioned above unsuitable and ineffective. Next, we provide a primer on the O-RAN architecture and discuss related work in conflict mitigation.

O-RAN—A Primer. The O-RAN architecture combines a disaggregated RAN with the RICs, deployed on an infrastructure composed of servers, hardware accelerators, and virtualization solutions, collectively referred to as the O-Cloud. Fig. 2 provides a logical diagram of this architecture. The disaggregated RAN features Next Generation Node Bases (gNBs) split into a Radio Unit (RU), Distributed Unit (DU), and Central Unit (CU), implementing different portions of the protocol stack. DUs and CUs are connected to the Near-RT RIC through the E2 interface, while all gNBs components connect to the network Service Management and Orchestration (SMO) framework via the O1 interface. The SMO embeds the Non-RT RIC, which connects to the Near-RT RIC via the A1 interface. More details on the O-RAN architecture are discussed in [1], [16].

Conflict Management in O-RAN. A systematic analysis of the challenges of conflict control in the RAN and of the strategies proposed to address them is presented in [5]. With respect to literature on conflicts in wireless systems, which primarily concerns the avoidance of interference in ad hoc networks [17], [18], the focus in [5] and in our paper is on avoiding conflicting configurations in the RAN protocol stack. Specifically, preventive conflict mitigation activities should reliably detect conflicts, also in a network with dynamic conditions, provide optimal conflict resolution and methodologies for testing, and evaluate conflict mitigation methods.

A conflict detection and mitigation framework for xApps at the Near-RT RIC is presented in [6]. Differently from PACIFISTA, this framework only detects conflicts on xApps already deployed on the O-RAN infrastructure. In light of the framework presented in [6], [7] proposes a Quality-of-Service Aware Conflict Mitigation method that identifies an optimal equilibrium point for all xApps while ensuring satisfaction of Quality of Service requirements. The framework, however, presents two potential areas for improvement, which the authors intend to address in future work. First, the framework is heavily dependent on KPM prediction, which is a complex task due to the dynamic and complex nature of the network. Secondly, it provides validation exclusively through Python-based simulated experiments based on a simplified model for the network KPM prediction.

A framework for orchestration of the deployment of O-RAN applications is presented in [4]. This framework performs conflict avoidance only by ensuring that conflicting applications are not concurrently deployed. However, this work does not perform conflict detection and mitigation, as

PACIFISTA instead does. A team learning-based strategy to reduce and eliminate conflicts among xApps in the Near-RT RIC is defined in [9]. In this approach, xApps learn to cooperate and avoid conflicts using a Deep Q-Network (DQN) architecture. However, this solution requires coordination during training, which might not always be the case in O-RAN, where multiple vendors publish their individually trained xApps and rApps. Building on this work, a case study of multi-agent team learning for xApps controlling different RAN parameters is presented in [8], where authors present a framework that mitigates conflicts in real-time, but does not reduce conflict occurrence by regulating xApp deployment, as PACIFISTA instead does.

In [19], the authors provide an overview of how conflicts can generate misconfigurations in O-RAN, and discuss how conflicts can impact all layers of the protocol stack and how this can result in increased energy consumption, performance degradation and instability. They also present a solution to detect conflicts but limit their study to direct and indirect conflicts, while mentioning that detection of implicit conflicts requires a more complex and data-driven solution, such as the one we present in this paper.

Lastly, [20] propose an approach based on neural networks to learn and construct graphs that describe conflicts.

Compared to the previous literature on the topic, our goal is to design and develop a full-fledged mathematical and operational framework that embeds pipelines to characterize individual O-RAN applications, and leverage statistical analysis to accurately evaluate the severity of conflicts and compute mitigation strategies both prior to O-RAN application execution, and at run time.

3 MODELING CONFLICTS IN O-RAN

3.1 Definitions of Conflicts

We introduce here the three classes of conflicts identified by the O-RAN Alliance [21].

- **Direct Conflicts** arise when applications control the same parameter (e.g., network slicing policies). An example of two applications controlling the same parameter p_2 is shown in Fig. 3a. For example, this occurs when two xApps both control network slicing policies (potentially with conflicting objectives).
- **Indirect Conflicts** occur when different applications control distinct parameters, but those parameters impact other parameters or KPMs and the interdependencies can be observed.
- **Implicit Conflicts** occur when different applications control distinct parameters, but those parameters impact other parameters or KPMs and the interdependencies can not be observed.

PACIFISTA’s graph-based approach to the problem of conflicts in O-RAN makes it logical to further classify indirect and implicit conflicts into two categories. This classification is not based on the observability of the effect of an application on parameters and KPMs, but rather on the structure of the graphs on which PACIFISTA’s analysis is based. Specifically, the two categories are:

- **Parameter Conflicts** occur when different applications control distinct parameters, but those parameters have interdependencies that cause undesired interactions.

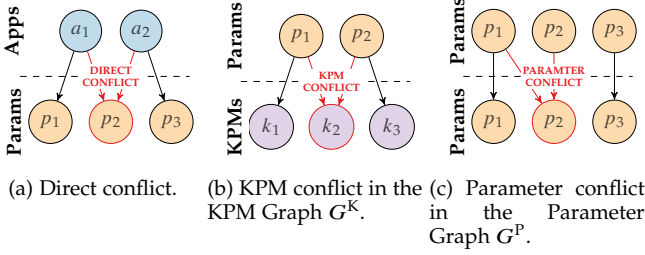


Fig. 3: Examples of conflicts and graphs used in PACIFISTA.

An example is an rApp powering off a base station and an xApp adjusting its transmission power. An example of parameter p_1 indirectly affecting parameter p_2 is shown in Fig. 3c.

- **KPM Conflicts** arise when different applications control separate parameters that target different KPM, but optimizing one metric can have unintended side effects on the metrics targeted by another application.

An example is that of an energy-saving rApp that jointly reduces bandwidth and transmission power to improve energy-efficiency, while an xApp requests high resource utilization to support video streaming applications. Intuitively, both applications will impact the throughput experienced by served users. The former will negatively impact throughput due to the reduction in achievable capacity of the cell, while the latter will use many spectrum resources to deliver the highest throughput. An example of two parameters affecting the same KPM k_2 is shown in Fig. 3b.

Implicit conflict detection assume no prior information on existence of conflicts, but this information can be built thanks to Machine Learning (ML) techniques that build knowledge about conflicts from available data, such as the one proposed in [20].

3.2 PACIFISTA's Conflict Model

We now introduce PACIFISTA's conflict model, as well as notation and graphs that will be used throughout the paper.

Let \mathcal{A} be the set of O-RAN applications that can be deployed on the RICs. For the sake of generality, in this work, we consider rApps, xApps and dApps, applications that extend O-RAN intelligence to the CUs and DUs [10]. Let \mathcal{P} be the set of parameters that can be controlled by applications in \mathcal{A} , and \mathcal{K} be the set of observable KPMs. For each application $a \in \mathcal{A}$ and parameter $p \in \mathcal{P}$, we define an indicator $\alpha_{a,p} \in \{0,1\}$ such that $\alpha_{a,p} = 1$ if application a controls parameter p , and $\alpha_{a,p} = 0$ otherwise. We can now define the set $\mathcal{P}^a = \{p \in \mathcal{P} : \alpha_{a,p} = 1\} \subseteq \mathcal{P}$ to identify the subset of parameters that are controlled by a . An illustrative example with two applications a_1 and a_2 , three parameters with $\mathcal{P}^{a_1} = \{p_1, p_2\}$ and $\mathcal{P}^{a_2} = \{p_2, p_3\}$ is shown in Fig. 3a.

KPM Graph G^K : this graph $G^K = (V^K, E^K)$ is shown in Fig. 3b and represents relationships between control parameters and KPMs. Nodes of G^K are both control parameters and KPMs, i.e., $V^K = \mathcal{P} \cup \mathcal{K}$, and edges E^K represent whether or not a control parameter $p \in \mathcal{P}$ impacts a certain KPM $k \in \mathcal{K}$. Any 2-tuple $(p, k) \in \mathcal{P} \times \mathcal{K}$ is an edge of G^K , i.e., $(p, k) \in E^K$ if and only if parameter p directly affects KPM

k . Let $\epsilon_{p,k} \in \{0,1\}$ be an indicator variable such that $\epsilon_{p,k} = 1$ if p impacts KPM k , and $\epsilon_{p,k} = 0$ otherwise. We define $E^K = \{(p, k) \in \mathcal{P} \times \mathcal{K} : \epsilon_{p,k} = 1\}$. In Fig. 3b, we show an example with two parameters (i.e., $\mathcal{P} = \{p_1, p_2\}$) and three KPMs (i.e., $\mathcal{K} = \{k_1, k_2, k_3\}$). p_1 impacts k_1 and k_2 , while p_2 impacts k_2 and k_3 . Since both p_1 and p_2 impact KPM k_2 , this causes a KPM conflict.

Parameter Graph G^P : this graph is illustrated in Fig. 3c and is used to represent relationships among control parameters. Specifically, nodes of G^P are $V^P = \mathcal{P}$ and edges E^P are used to represent dependencies between parameters. For any 2-tuple $(p_1, p_2) \in \mathcal{P} \times \mathcal{P}$, let $\pi_{p_1, p_2} \in \{0,1\}$ be an indicator parameter such that $\pi_{p_1, p_2} = 1$ if parameter p_1 impacts parameter p_2 , $\pi_{p_1, p_2} = 0$ otherwise. This graph aims at capturing dependencies between parameters and their respective conflicts, especially in those cases where the value of a parameter p_1 affects directly the value that p_2 can take as shown in Fig. 3c. For example, in the case that p_1 is used to turn off a base station, and p_2 represents its transmission power, then $p_2 = 0$ if the base station is off (i.e., $p_1 = 0$). Formally, we have $E^P = \{(p_1, p_2) \in \mathcal{P} \times \mathcal{P} : \pi_{p_1, p_2} = 1\}$.

As we will discuss in Section 6, the graph described above are used to identify relationships between applications, parameters and KPMs, and are used to determine which applications can potentially generate conflicts. However, in Section 7, we show that severity of conflicts depends on operational conditions. Therefore, while the indicators and graphs described above show the potential of conflict occurrence, the relevance of such conflicts will be evaluated in each operational condition.

These graphs can be built using the concept of causality [22], which allows to determine how a certain variable directly impacts the value of another variable. In this case, it makes it possible to determine direct causality relationships from observational data, and such relationships are represented via a directed graph [22].

Given the O-RAN definitions of conflicts provided in Section 3.1, and the notations introduced before, we formally define these conflicts as follows. Since indirect and implicit conflicts only differ with respect to availability of knowledge, which can be built using [20], in the following we consider them together and focus on their parametric and KPM sub-classification.

Definition 1 (Direct Conflict). Let $p \in \mathcal{P}$ be any parameter. Let a_1 and a_2 be any two applications in \mathcal{A} . We say that a_1 and a_2 are in direct conflict with respect to parameter p if $p \in \mathcal{P}_{a_1, a_2}^{DC} = \mathcal{P}_{a_1} \cap \mathcal{P}_{a_2}$.

Definition 2 (Parameter Conflict). Let a_1 and a_2 be any two applications in \mathcal{A} . We say that parameter $p_1 \in \mathcal{P}_{a_1}$ controlled by application a_1 generates a Parameter conflict with parameter $p_2 \in \mathcal{P}_{a_2}$ controlled by a_2 if $(p_1, p_2) \in E^P$, i.e., $\pi_{p_1, p_2} = 1$.

Definition 3 (KPM Conflict). Let a_1 and a_2 be any two applications in \mathcal{A} . We say that a_1 and a_2 generate a KPM conflict with respect to KPM $k \in \mathcal{K}$ if there exists at least one 2-tuple $(p_1, p_2) \in \mathcal{P}_{a_1} \times \mathcal{P}_{a_2}$, with $p_1 \neq p_2$ such that $\epsilon_{p_1, k} = \epsilon_{p_2, k} = 1$.

4 PACIFISTA OVERVIEW

PACIFISTA has a modular architecture (Fig. 2) with four major logical blocks and a catalog of applications (e.g., rApps, xApps and dApps). In this section, we will give a high-level overview of these blocks, while their detailed description will be given in Sections 5-8.

4.1 PACIFISTA in a Nutshell

PACIFISTA executes four major tasks, namely application profiling, conflict detection, evaluation, and mitigation. The *Profiler* runs on sandbox testing environments (e.g., digital twins, emulation environments) and generates profiles that describe the statistical behavior of O-RAN applications. This process will be detailed in Section 5.1. The *Conflict Detection Module* uses such profiles for detecting the occurrence of conflicts and identifying the affected parameters and KPMs. Upon detecting the existence of conflicts, the *Conflict Evaluation Module*, which is executed on the production network, generates a report that summarizes how severe the conflict is, and how much it impacts the KPMs. Finally, the *Conflict Mitigation Module* leverages the information included in the report to make informed decisions on the deployment of O-RAN applications. These decisions are made by using conflict management policies specified by the network operator, such as avoiding the deployment of an application that would generate too large of a conflict, or removing a subset of applications to reduce the severeness of conflicts below a certain threshold.

4.2 Integration with O-RAN

As shown in Fig. 2, PACIFISTA runs as a component of the SMO, and it leverages its internal messaging infrastructure to access the O1 termination and to interface with the RICs and RAN nodes (e.g., CUs and DUs). It is worth noticing that PACIFISTA only needs to get access to application deployment and removal procedures. Following O-RAN specifications [1], this only requires access to the O1 interface. The profiling process, described in Section 5.1, happens offline and consists of evaluating applications in one or more of the sandbox environments in Fig. 2 (e.g., a digital twin or an isolated/test segment of the network). Each application is associated with a set of application profiles, one per operational condition. Each operational condition specifies the wireless environment characteristics (e.g., channel conditions), traffic demand, mobility, and location of nodes that will be experienced by the application (e.g., xApp) upon deployment. This information is not used by PACIFISTA for its computations, but it is solely recorded to distinguish the different operational scenarios in which the applications considered work.

First, PACIFISTA gathers raw data and statistics on the decisions rApps, xApps, and dApps make based on the live KPMs they get from the RAN nodes directly (dApps), through the E2 interface (xApps), and the O1 interface (rApps). Then, PACIFISTA performs profiling operations through statistical analysis on collected data by extracting Empirical Cumulative Density Functions (ECDFs) for parameters and KPMs, and generates the application profiles to be included in the catalog.

As we will describe in Section 8, the operator can specify conflict management policies that are used to determine

which rApps, xApps, and dApps can be deployed on the RICs depending on the level of conflict they generate. Once PACIFISTA makes a decision on the subset of O-RAN applications to deploy, the O1 interface is used to deploy xApps on the Near-RT RIC and dApps in RAN nodes, while the internal messaging infrastructure of the SMO is used to deploy rApps on the Non-RT RIC. In both cases, applications are instantiated from a catalog hosted in the SMO. Similarly, existing applications can be removed by PACIFISTA in case they would conflict with new applications that need to be instantiated. The O-RAN interfaces also enable PACIFISTA to manage and monitor applications that have already been deployed. As an example, the O1 and the R1 interfaces can be used to perform health checks on the status of the running applications, or to tune their configuration.

5 PROFILING O-RAN APPLICATIONS

The *Catalog* hosts rApps, xApps, and dApps that can be deployed on an O-RAN network. For each application $a \in \mathcal{A}$, the catalog stores an *application profile* consisting of the following components:

- **Identifier:** used to uniquely identify each application.
- **Parameter set:** this field specifies the list of parameters *directly* controlled by the application (i.e., \mathcal{P}_a).
- **Statistical profile:** it provides statistical information on the behavior of the application under certain operational conditions. We consider the case where applications are profiled on a set C of predefined operational conditions. Each operational condition $c \in C$ can specify, among others, the number of User Equipments (UEs), cell load, Signal to Interference plus Noise Ratio (SINR)/Channel Quality Information (CQI) conditions. This information is available to operators via real-time and historical data. For each c , we store the statistical profile of the application which includes Probability Density Functions (PDFs), Cumulative Distribution Functions (CDFs), and ECDFs used to characterize how application a configures the parameters in \mathcal{P}_a when operating under conditions c . In this paper, we use ECDFs as these are model-free and can be extracted directly from data.

Remark 1. To properly capture conflicts in O-RAN, it is important to notice that conflicts are strongly dependent on operational conditions. It is generally incorrect to state that two applications always generate conflicts. Indeed, two applications a_1 and a_2 might heavily conflict with each other under operational conditions c_1 , but their conflict may be negligible under conditions c_2 . For this reason, PACIFISTA captures the statistical behavior of each application across C and evaluates conflicts for each operational condition of interest. Moreover, the statistical profiling methodology employed by PACIFISTA is based on the assumption that there will be a certain level of noise and outliers. In order to account for these factors, the applications are executed for an extended period of time within the sandbox environment. This allows the collection of sufficient data to generate statistically valid results that include the noise and the possible outliers. It should be noted that outliers are not erroneous decisions; rather, they are decisions that do not follow the expected distribution. The presence of a significant number of outliers indicates that the generated

profile does not align well with the curve of the real-world scenario, and it is necessary to create a new profile for that specific operational condition.

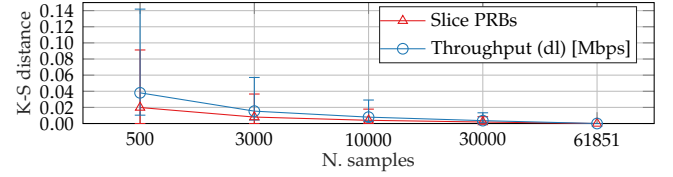
Remark 2. The parameter set is provided to the network operator by the application developer via a manifest. Among others, the manifest defines inputs and outputs of the algorithm implemented in the application, E2 service models required to run the model, controllable parameters and required KPMs.

5.1 Creating Statistical Profiles

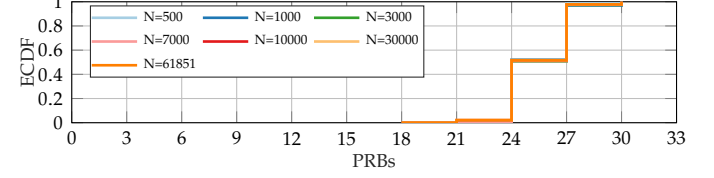
The creation of the statistical profiles is one of the most important aspects of PACIFISTA as they allow it to detect and evaluate conflicts for mitigation and management. In PACIFISTA, we generate statistical profiles by executing sandbox testing operations under each condition specified in C . In this context, “sandbox” refers to an environment that simulates (or emulates) real-world network conditions and allows testing of O-RAN applications, network configurations, protocols, and services in a controlled virtual (e.g., digital twin) or physical (e.g., anechoic chamber) environment.

To generate accurate application profiles, it is necessary to collect enough samples to achieve statistical relevance for each operational condition, application and scenarios. Indeed, statistical relevance varies across scenarios and applications. Therefore, the number of samples required to collect in each case is a design parameter that balances computational complexity with desired level of accuracy. With respect to the applications considered in our experimental analysis (shown in Section 9), we collected at least 3,000 samples for each xApp for each slice. Fig. 4 shows how the application profile changes with the number of samples evaluated for slice Massive Machine-Type Communications (mMTC) (similar results were obtained for other slices and xApps). Fig. 4b and 4c show how the profiles for the variables considered are very similar, despite the vast range of samples analyzed. Fig. 4a shows how the Kolmogorov-Smirnov (K-S) distance (more on this metric in Section 7) between each sample size and the total number of samples collected is very small (< 0.02 for the distance between the profile built with 3,000 and $> 60,000$ samples). This means that the error on distance values due to having collected $\sim 3,000$ samples instead of $> 60,000$ is lower than 0.02. Despite this being an acceptable error for the purpose of these experiments, we still used all the data available to build the profiles of each application. Moreover, the accuracy of the application profiles depends on how accurate the sandbox testing environment is. The more accurate the sandbox environment (e.g., the digital twin), the more accurate the application profile. Finally, since applications behave differently under different operational conditions, PACIFISTA generates an application profile for each operational condition to accurately capture conflicts under different deployments. In our implementation of PACIFISTA (see Section 9), operational conditions have been specified by the number of base stations and their deployment location, the total number of UEs, their mobility pattern, distribution, and traffic profiles.

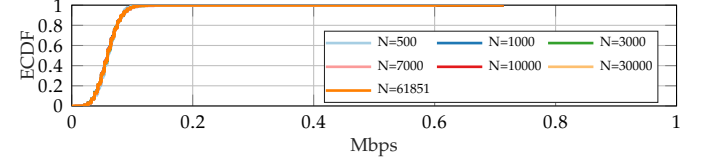
In this work, we achieve this by using the Colosseum O-RAN digital twin [23] and the OpenRAN Gym open-



(a) K-S distance among different samples sizes and the total number of samples collected for xApp a_5 .



(b) ECDF of assigned PRBs for different samples sizes for xApp a_5 .



(c) ECDF of downlink throughput for different samples sizes for xApp a_5 .

Fig. 4: Application profile comparison for different number of samples for slice mMTC of xApp a_5 .

source O-RAN framework [11]. This procedure is illustrated in Fig. 5 and described below.

Step 1: This step consists in *creating testing scenarios* to be included in C and to be used as benchmarks to evaluate conflicts. These are generated according to the availability of the O-RAN testing environment. Digital twins, network emulators, and testing equipment (e.g., RIC, RAN testers) are ideal platforms as these are controllable and reproducible environments. However, this does not exclude the use of over-the-air experimental platforms, lab setups, as well as portions of production networks. In this work, we leverage Colosseum to generate cellular scenarios by specifying topology (i.e., extracted from GPS coordinates from OpenCellID [24]), RF conditions (e.g., multi-path, fading), mobility, and traffic profiles, among others. Details on these scenarios will be given in Section 9. Note that an application $a \in \mathcal{A}$ can only control \mathcal{P}_a , and those not controlled by a , i.e., $\mathcal{P}_{-a} = \mathcal{P} \setminus \mathcal{P}_a$, can assume multiple values. For this reason, we assume that each testing scenario c also specifies the values of parameters in \mathcal{P}_{-a} . In this way, we can benchmark the same application a across multiple testing scenarios that have the same topology, RF conditions, mobility and traffic profiles, but have different parameter configurations.

Step 2: We select an application $a \in \mathcal{A}$ and *execute*

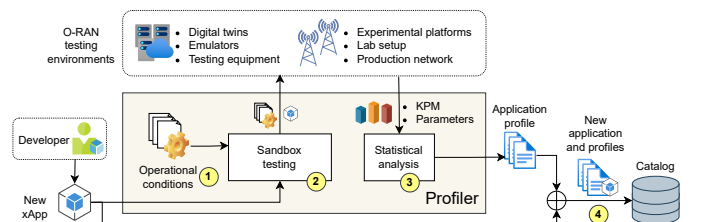


Fig. 5: Profiling of new O-RAN applications.

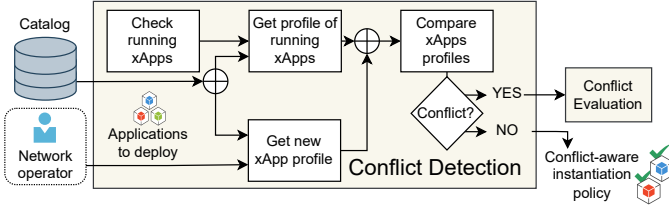


Fig. 6: Conflict detection module and interactions with other modules.

sandbox tests under testing scenario $c \in C$. PACIFISTA collects and logs data transmitted over O-RAN interfaces (e.g., O1, E2, A1) such as KPMs \mathcal{K} , control parameters \mathcal{P} and enrichment information. We store both parameters controlled by a and those that are not. Note that parameters in \mathcal{P}_{-a} can be either fixed (e.g., assuming their default value), or change dynamically due to deterministic policies or due to other applications controlling them. In this latter case, where tests involve multiple applications executing at the same time (e.g., an xApp a_1 and an rApp a_2), we treat such applications as a “virtual” application a controlling $\mathcal{P}_a = \mathcal{P}_{a_1} \cup \mathcal{P}_{a_2}$.

Step 3: PACIFISTA processes the data generated in the previous step to produce the statistical profile that describes the control behavior of application a under testing scenario c , and the subsequent impact on KPMs. In general, one could also store the original raw data in the statistical profile. However, this might be impractical due to its sheer size.¹ For this reason, we have designed our conflict evaluation pipeline to only require statistical information of data, i.e., CDFs of KPMs, while raw data is stored in data lakes.

Step 4: Once statistical profiles have been generated, they are attached to application a and published to the catalog.

6 DETECTING CONFLICTS

The first step in conflict mitigation consists in detecting the occurrence of conflicts. The *Conflict Detection Module* takes as input the set of applications $\mathcal{A}^* \subseteq \mathcal{A}$ that the operator wants to deploy² and (i) identifies the subset of applications that will generate conflicts; and (ii) identifies the set of parameters and KPMs that will be impacted. Fig. 6 shows how the Conflict Detection module works. Specifically, PACIFISTA first extracts application profiles from the catalog, then compares the profiles to identify conflicts as described in the following sections. Ultimately, if no conflicts are detected, the applications are deployed directly. Otherwise, detected conflicts are sent to the conflict evaluation module described in Section 7.

6.1 Detecting Direct Conflicts

Following from Definition 1, the set \mathcal{P}^{DC} of parameters suffering from direct conflicts with respect to the application

1. A single benchmark on our prototype generates 1.66 Mbps/gNB of data when serving 6 UEs and storing more than 30 KPMs for each one of them.

2. In practical applications, this set can be represented as $\mathcal{A}^* = \mathcal{A}^{\text{new}} \cup \mathcal{A}^{\text{old}}$, where \mathcal{A}^{new} and \mathcal{A}^{old} are the set of new applications that need to be deployed and the set of applications that are already deployed, respectively.

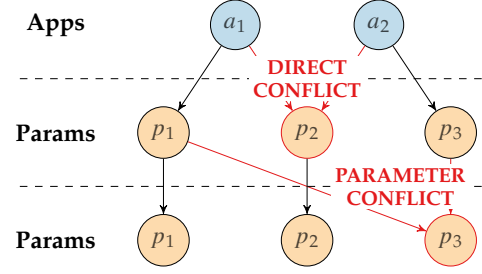


Fig. 7: Augmented graph $G^{\mathcal{P}}$ to detect direct (p_2) and parameter (p_3) conflicts.

set \mathcal{A}^* is

$$\Pi^{\text{DC}}(\mathcal{A}^*) = \left\{ p \in \bigcup_{a \in \mathcal{A}^*} \mathcal{P}_a : \sum_{a \in \mathcal{A}^*} \alpha_{a,p} > 1 \right\}. \quad (1)$$

To identify these parameters, we augment the Parameter Graph $G^{\mathcal{P}}$ by adding an extra layer above that represents the applications in \mathcal{A}^* . Specifically, we add as many nodes as applications in \mathcal{A}^* and generate any edge $(a, p) \in \mathcal{A}^* \times \mathcal{P}$ such that $\alpha_{a,p} = 1$.

Fig. 7 shows an example of this graph, which PACIFISTA also uses to identify Parameter conflicts (see Section 6.2) with two applications and a total of three controllable parameters. Application a_1 controls p_1 and p_2 , while a_2 controls p_2 and p_3 . Fig. 7 shows how the two applications generate a direct conflict with respect to p_2 as this parameter has more than one incoming edges. For each parameter $p \in \Pi^{\text{DC}}(\mathcal{A}^*)$, we also identify the subset of applications in \mathcal{A}^* that generate a direct conflict on p as follows:

$$\Theta_p^{\text{DC}}(\mathcal{A}^*) = \{ a \in \mathcal{A}^* : \alpha_{a,p} = 1 \}. \quad (2)$$

In Fig. 7, we have that $\Pi^{\text{DC}}(\mathcal{A}^*) = \{ p_2 \}$ and $\Theta_{p_2}^{\text{DC}}(\mathcal{A}^*) = \{ a_1, a_2 \}$.

6.2 Detecting Parameter Conflicts

From Definition 2, and by using the augmented graph built in Section 6.1 and illustrated in Fig. 7, parameter conflicts can be characterized by identifying the following two sets:

$$\Pi^{\text{PC}}(\mathcal{A}^*) = \left\{ p \in \bigcup_{a \in \mathcal{A}^*} \mathcal{P}_a : \sum_{p' \in \bigcup_{a \in \mathcal{A}^*} \mathcal{P}_a} \pi_{p',p} > 1 \right\}, \quad (3)$$

$$\Theta_p^{\text{PC}}(\mathcal{A}^*) = \{ a \in \mathcal{A}^* : \alpha_{a,p} = 1 \} \quad (4)$$

for each parameter $p \in \Pi^{\text{PC}}(\mathcal{A}^*)$. From Fig. 7 (bottom part), we notice that parameter p_3 depends on p_1 , i.e., $\pi_{p_1,p_3} = 1$. Since $p_1 \in \mathcal{A}_{a_1}$, we have that decisions taken by a_1 inadvertently affect the value of parameters controlled by a_2 , which is a Parameter conflict.

6.3 Detecting KPM Conflicts

KPM conflicts are defined in Definition 3. Despite these conflicts being harder to model as they depend on intrinsic relationships between control parameters and observable KPMs, they can be detected using a procedure that is similar to that used for Parameter conflicts. Specifically, we augment the graph $G^{\mathcal{K}}$ by adding nodes such that each node a represents an application in \mathcal{A}^* . Moreover, we also add edges $(a, p) \in \mathcal{A}^* \times \mathcal{P}$ such that $\alpha_{a,p} = 1$.

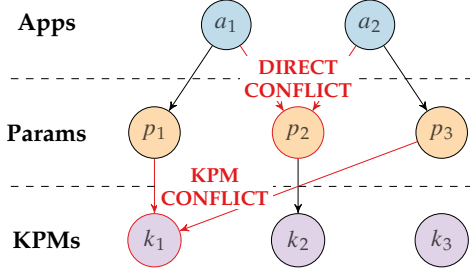


Fig. 8: Augmented graph G^K to detect KPM conflicts (k_1). The graph also shows a direct conflict at p_2 .

Fig. 8 shows an example of this graph. We can detect KPM conflicts by identifying which KPM nodes have more than one incoming edge. In this example, a_1 controls $\{p_1, p_2\}$, a_2 controls $\{p_2, p_3\}$. While the two applications generate a direct conflict on p_2 , we notice that k_1 depends on both p_1 and p_3 . As the two applications control both parameters, k_1 is affected by a parameter conflict. KPM conflicts can be identified via the following two sets:

$$\Pi^{\text{KC}}(\mathcal{A}^*) = \left\{ k \in \mathcal{K} : \sum_{p \in \bigcup_{a \in \mathcal{A}^*} \mathcal{P}_a} \epsilon_{p,k} > 1 \right\}, \quad (5)$$

$$\Theta_p^{\text{KC}}(\mathcal{A}^*) = \{ a \in \mathcal{A}^* : \alpha_{a,p} = 1 \} \quad (6)$$

for each parameter $p \in \Pi^{\text{KC}}(\mathcal{A}^*)$.

7 EVALUATING CONFLICTS

Another important aspect of conflict management in O-RAN is that of conflict severity. This is particularly important as some conflicts might happen frequently, but their impact on network performance and efficiency might be tolerable under certain conditions. The Conflict Evaluation Module in Fig. 9 analyzes each conflict detected in the previous phase over the application set \mathcal{A}^* , and outputs a conflict report containing a set of indexes that measure the severity of conflicts and their potential impact on network performance. In our prototype, this procedure takes approximately twenty seconds. In the following, we introduce a set of metrics that we use in PACIFISTA to characterize conflicts, as well as methods to compute them via PACIFISTA's Conflict Evaluation Module.

In Tab. 1, we summarize the metrics used by PACIFISTA to provide an assessment of the severity of conflicts between O-RAN applications. To simplify the notation, we provide their general definition for two one-dimensional generic ECDFs $F_1(x)$ and $F_2(x)$ with $x \in \mathbb{R}$ being a random variable. In our analysis, we have compared several distance metrics

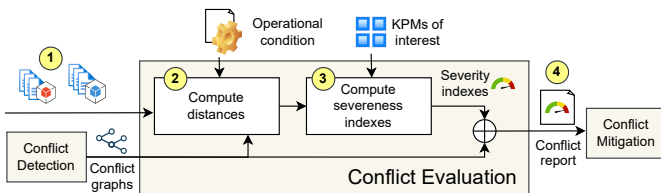


Fig. 9: Conflict evaluation module and interactions with other modules.

TABLE 1: Distance functions used in PACIFISTA to evaluate conflicts in O-RAN.

ID	Equation	Description
K-S	$\max F_1(x) - F_2(x) $	Maximum vertical distance between the two ECDFs.
INT	$\sqrt{\frac{1}{L} \int F_1(x) - F_2(x) }$	Integral of the absolute value of the distance between the two ECDFs, with $L = \max(x) - \min(x)$.
χ	$1 - p\text{-value}$	Likelihood that data from two categorical distributions are different.

to identify the most suitable ones for the purpose of conflict evaluation. Specifically, we have selected K-S and Integral Area (INT) for all numerical variables. As we will show in Section 9.2, the K-S distance is suitable for detecting conflicts, since the values of K-S distance are often close or equal to 1 in the case of conflict, and they are not as high otherwise. However, these K-S distances are not easily comparable as they only account for vertical distance between two ECDFs, which does not provide insights on how different the two distributions are. On the contrary, the INT distance, which quantifies the area between two distributions, takes values that are more uniformly distributed in the $[0, 1]$ interval. For this reason, the INT distance is convenient for making comparisons and measuring conflict severity. Fig. 10 shows a graphical representation of the two distances. In case of categorical variables, PACIFISTA uses the Pearson's Chi-Square test, where the distance between two applications is measured using the resulting p -value [25], as indicated in Tab. 1. By definition, all distances we consider take values in $[0, 1]$.

PACIFISTA uses ECDFs, which provide an accurate data-driven representation of the decision-making of each application for a certain operational condition $c \in \mathcal{C}$. The evaluation process in PACIFISTA is executed as follows:

Step 1: We select two applications a' and a'' and retrieve their statistical profile. We also select an operational condition $c \in \mathcal{C}$ of interest. For each $p \in \mathcal{P}_{a'} \times \mathcal{P}_{a''}$, we extract the ECDFs of the two applications with respect to p , say $F_{a'}(p|c)$ and $F_{a''}(p|c)$.

Step 2: We use Tab. 1 to compute the distance between $F_{a'}(p|c)$ and $F_{a''}(p|c)$ for each $p \in \mathcal{P}_{a'} \times \mathcal{P}_{a''}$. We refer to this distance as $D_{a',a''}^f(p|c)$, where f represents the specific metric used to compute the distance as identified in Tab. 1. For example, $D_{a',a''}^{\text{K-S}}(p|c)$ represents the Kolmogorov-Smirnov (KS) distance between applications a' and a'' with respect to control parameter p under operational conditions

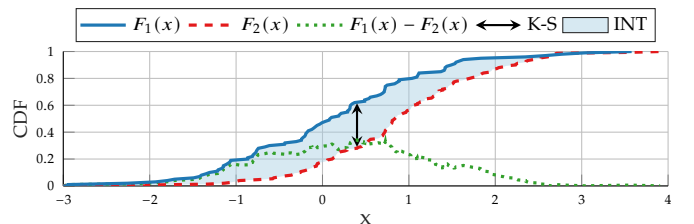


Fig. 10: Graphical representation of the different distance metrics.

c . Similarly, for each $k \in \mathcal{K}$, we extract the ECDFs of a' and a'' with respect to KPM k . With a slight abuse of notation, we denote these ECDFs as $F_{a'}(k|c)$ and $F_{a''}(k|c)$, respectively.

Step 3: We compute the distance between $F_{a'}(k|c)$ and $F_{a''}(k|c)$ for each $k \in \mathcal{K}$ via Tab. 1. We use $D_{a',a''}^f(k|c)$ to indicate the distance between a' and a'' with respect to KPM k , under conditions c and for a certain distance metric with identifier f (from Tab. 1).

Step 4: We combine the above distance metrics with respect to f to generate two arrays $\mathbf{D}_{a',a''}^f(\mathcal{P}, c) = (D_{a',a''}^f(p|c))_{p \in \mathcal{P}}$ and $\mathbf{D}_{a',a''}^f(\mathcal{K}, c) = (D_{a',a''}^f(k|c))_{k \in \mathcal{K}}$. $\mathbf{D}_{a',a''}^f(\mathcal{P}, c)$ describes how applications a' and a'' differ in terms of decision making policies (e.g., how differently they control the same set of parameters), while $\mathbf{D}_{a',a''}^f(\mathcal{K}, c)$ describes how the applications impact KPMs as a consequence of their different behavior. Both $\mathbf{D}_{a',a''}^f(\mathcal{P}, c)$ and $\mathbf{D}_{a',a''}^f(\mathcal{K}, c)$ are processed to generate a detailed report describing conflicts between a' and a'' . The report contains information regarding the existence of direct, parameter and KPM conflicts, statistical information detailing how conflicts impact KPMs and parameters, as well as a set of indexes that are used by PACIFISTA to express the severity of each conflict. The format of the report and the information contained therein will be described in Section 7.1.

7.1 The Conflict Report

PACIFISTA leverages the information produced so far to generate the *conflict report*. The objective of this report is twofold: (i) identify the existence of any type of conflict; and (ii) provide augmented information on how severe these conflicts are with respect to operators' objectives. Its generation is illustrated in Fig. 9.

Operators can also specify the subset \mathcal{P}^* and \mathcal{K}^* of parameters and KPMs that are relevant to operator's goals and should be therefore considered when mitigating conflicts. For example, throughput might be an important KPM for eMBB applications, but be less relevant for Ultra Reliable and Low Latency Communications (URLLC) traffic. For a given set \mathcal{A}^* of applications to be evaluated, and sets \mathcal{P}^* and \mathcal{K}^* , the report contains the following elements:

- **Conflict Existence:** the first elements included in the report are the sets $\Pi^{\text{DC}}(\mathcal{A}^*)$, $\Pi^{\text{PC}}(\mathcal{A}^*)$, $\Pi^{\text{KC}}(\mathcal{A}^*)$, $\Theta_p^{\text{DC}}(\mathcal{A}^*)$, $\Theta_p^{\text{PC}}(\mathcal{A}^*)$, and $\Theta_p^{\text{KC}}(\mathcal{A}^*)$ for each parameter $p \in \mathcal{P}$ as defined in (1)-(6). These identify types of conflicts, which applications cause them and affected parameters and KPMs. PACIFISTA also includes the augmented graphs (Section 6) used to visualize conflicts (Fig. 7).
- **Conflict Severity:** for a given set \mathcal{A}^* of applications of interest with cardinality A^* , we have a total of $A^*(A^* - 1)/2$ conflict pairs.³ For each pair, PACIFISTA computes two severity indexes $\sigma_{a',a''}^{\mathcal{P}}(\mathcal{P}^*|c)$ and $\sigma_{a',a''}^{\mathcal{K}}(\mathcal{K}^*|c)$. Each index summarizes how severe the different types of conflicts are by aggregating the distances $D_{a',a''}^f(z|c)$ computed in Tab. 1 for

variable $z \in \mathcal{P}^*$ or $z \in \mathcal{K}^*$ under operational condition c into a single value.

To combine the above distances and generate severity indexes for any given condition c and distance metric f , we use a combining function $H(\cdot)$ such that $\sigma_{a',a''}^{\mathcal{P}}(\mathcal{P}^*|c) = H(\mathbf{D}_{a',a''}^f(\mathcal{P}^*, c))$ and $\sigma_{a',a''}^{\mathcal{K}}(\mathcal{K}^*|c) = H(\mathbf{D}_{a',a''}^f(\mathcal{K}^*, c))$. Although $H(\cdot)$ can take any form, suitable aggregator functions for an N -dimensional array $\mathbf{x} = (x_1, \dots, x_N)$ are average (i.e., $H(\mathbf{x}) = 1/N \sum_{i=1}^N x_i$), median and maximum (i.e., $H(\mathbf{x}) = \max\{x_1, \dots, x_N\}$) operators.

It is worth mentioning that PACIFISTA computes the severity indexes based on the specific operational condition c . This is important as applications might generate conflicts only under certain conditions, and the severity of such conflicts might vary considerably under diverse operational conditions. For this reason, in PACIFISTA operators need to specify the operational conditions of interest prior to generating a report.

8 MITIGATING CONFLICTS

In practical deployments, conflicts can occur with non-zero probability due to coupling between control parameters and KPMs, limited amount of resources that result in competition between users, as well as conflicting intents (e.g., energy minimization against demand for high performance). This means that operators either decide to deploy a handful of applications that can act in concert and serve a few types of subscribers to deliver specific services, or need to tolerate a certain degree of conflict. The first approach minimizes the occurrence of conflicts, but it also makes it difficult to satisfy performance requirements for a variety of services and applications. For this reason, we consider the second approach to showcase how the conflict evaluation of PACIFISTA can be effectively used for more intelligent and dynamic conflict mitigation.

PACIFISTA implements a threshold-based conflict mitigation strategy, where the tolerance level δ^{TOL} is used to identify applications that would generate too high a conflict and should not be deployed at that time. In PACIFISTA, operators set a certain level of conflict tolerance δ^{TOL} , which specifies the maximum level of conflict that the operator is willing to tolerate when deploying O-RAN applications. Since both K-S and INT assume values in $[0, 1]$ and represent distances between ECDFs, they are unitless. Therefore, $\delta^{\text{TOL}} \in [0, 1]$ is also unitless. The operator can also submit a priority index I_a for each application $a \in \mathcal{A}$, which reflects the importance the operator assigns to each application and is used by PACIFISTA to determine which application to prioritize in the event of conflicts. δ^{TOL} can be fixed for all deployment cycles, or set dynamically to a new value each time PACIFISTA is run for a new group of applications. δ^{TOL} can also be specified as an array of thresholds for each KPM for each slice. Each entry is between 0 and 1, and is equal to 1 if the network operator does not have an interest in monitoring that specific KPM. This allows the operator to have a more fine-grained control over the behavior of the network. In the following reasoning, it is assumed that the operator only provides a single threshold to be compared to the severity indices, which are a summary of the conflict level on the single KPM.

3. Note that the commutative property applies to conflict evaluation, i.e., evaluating the conflict for the pair (a', a'') returns the same values as the evaluation for (a'', a') .

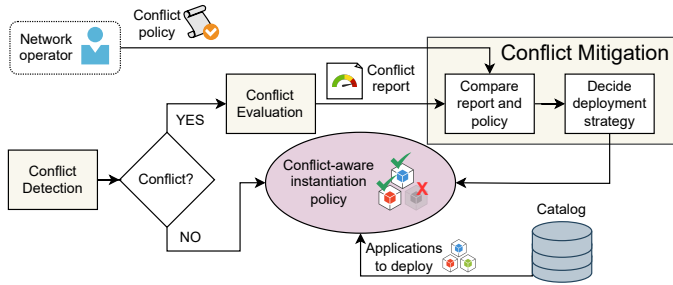


Fig. 11: Conflict mitigation module and interactions with other modules.

Upon receiving the set \mathcal{A}^* of applications to evaluate, the conflict mitigation module compares the severity indexes $\sigma_{a',a''}^P(\mathcal{P}^*|c)$ and $\sigma_{a',a''}^K(\mathcal{K}^*|c)$ (computed in Section 7.1) with the conflict threshold to determine which O-RAN applications to deploy to mitigate the occurrence of conflicts. Specifically, since operators are more interested in tolerating conflicts with respect to their impact on KPMs rather than on parameter configurations, in the following we focus on $\sigma_{a',a''}^K(\mathcal{K}^*|c)$.

The procedures involved in our threshold-based algorithm, shown in Fig. 11, are as follows:

Step 1: PACIFISTA identifies all the applications in \mathcal{A}^* that can be deployed without generating any type of conflict. These applications are added to a set $\mathcal{A}^{\text{DPLY}}$ of applications to deploy, which is initially set to $\mathcal{A}^{\text{DPLY}} = \emptyset$.

Step 2: We select the application with the highest priority from $\mathcal{A}^* \setminus \mathcal{A}^{\text{DPLY}}$, i.e., $a = \arg \max_{a \in \mathcal{A}^* \setminus \mathcal{A}^{\text{DPLY}}} \{I_a\}$. We add a to $\mathcal{A}^{\text{DPLY}}$ if $\max_{a^* \in \mathcal{A}^{\text{DPLY}}} \{\sigma_{a,a^*}^K(\mathcal{K}^*|c)\} \leq \delta^{\text{TOL}}$. We update $\mathcal{A}^* = \mathcal{A}^* \setminus a$.

Step 3: We repeat Step 2 until $\mathcal{A}^* = \emptyset$.

The above procedure can also be extended to the onboarding of new applications, that is when deploying new applications when other applications have already been deployed. In this case, we set $\mathcal{A}^{\text{DPLY}} = \mathcal{A}^{\text{old}}$.

9 EXPERIMENTAL EVALUATION

In this section, we first describe PACIFISTA's prototype, and then present experimental results that illustrate how PACIFISTA can be used to identify, characterize and mitigate conflicts in O-RAN.

9.1 Prototype Description

PACIFISTA has been prototyped on the OpenRAN Gym framework [11] and tested experimentally on the Colosseum wireless network emulator [23], which enables at-scale experimentation with Software-defined Radios (SDRs) as well as with realistic and heterogeneous Radio Frequency (RF) scenarios representative of real-world deployments. Specifically, we leveraged the SCOPE and CoIO-RAN components of OpenRAN Gym [11] to instantiate a cellular network with a softwarized base station and 6 UEs, and to deploy Near-RT RIC and xApps that interface with the base station through the O-RAN E2 termination. We use this as a sandbox environment to test a diverse set of xApps, collect data on their decision-making, and create statistical profiles of conflicts.

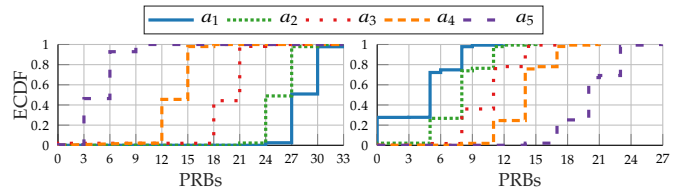


Fig. 12: ECDFs of eMBB (left) and URLLC (right) PRB allocation for a_1 - a_5 .

To fairly compare all xApps against the same repeatable operational conditions c , we benchmark them on the Rome Colosseum scenario [11]—which reproduces the real-world cellular deployment in a section of Rome, Italy. We consider 6 UEs uniformly distributed within 50 m from the Base Station (BS), which allocates them in three network slices (eMBB, URLLC, and mMTC) across 10 MHz of spectrum (50 PRBs grouped into 17 Resource Block Groups (RBGs)). We leveraged the Multi-Generator (MGEN) [26] tool to serve downlink traffic to the slice UEs as follows: (i) eMBB UEs are served constant bit rate traffic at a rate of 4 Mbps; (ii) URLLC are served Poisson-distributed traffic at an average rate of 89.29 kbps; and (iii) mMTC UEs are served Poisson-distributed traffic at an average rate of 44.64 kbps.

Our xApps act on a combination of two control parameters: (i) the *network slicing policy*, by adjusting the number of PRBs allocated to each slice; and (ii) the *scheduling policy* used in downlink transmissions, chosen among Waterfilling (WF), Round Robin (RR), and Proportional Fair (PF). Although PACIFISTA is general and can be used to profile any O-RAN application that embeds logic to control RAN parameters, in our experimental evaluation we focus on two classes of xApps: stochastic and Deep Reinforcement Learning (DRL)-based xApps. Stochastic xApps embed predictable decision-making logic that will be used to showcase PACIFISTA functionalities, and highlight the importance of identifying and characterizing conflicts. DRL-based xApps include a selection of xApps taken from the literature [27] and embed DRL agents trained to satisfy intents and diverse slice requirements.

9.1.1 Stochastic xApps (a_1 - a_5)

This set includes 5 xApps controlling slicing policies generated via a Gaussian distribution with different mean values per slice and a standard deviation of 1.5. xApps execute in real time and generate a new random slicing policy every 250 ms based on the distribution assigned to the xApp. Each new PRB assignment policy is generated by drawing a value for each slice around the mean value of the PRB distribution for the slice with a variance of 1.5. Prior to transmission, each random draw is rounded to the closest RBGs allocation, and then the policy is checked to avoid allocating more than the 50 available PRBs. ECDFs for xApps a_1 - a_5 and slices eMBB and URLLC are shown in Fig. 12. We omit the ECDF for slice mMTC, which receives the remaining PRBs.

9.1.2 DRL-based xApps (a_6 - a_8)

These xApps are taken from [27] and embed DRL agents controlling a combination of slicing (i.e., the portion of the available PRBs allocated to each slice) and scheduling (i.e.,

TABLE 2: K-S (Left) and INT (Right) distances for eMBB with respect to xApp a_1 . The last row shows the severity index for the corresponding xApp comparison.

	$D_{1,2}^{K-S}$	$D_{1,3}^{K-S}$	$D_{1,4}^{K-S}$	$D_{1,5}^{K-S}$	$D_{1,2}^{INT}$	$D_{1,3}^{INT}$	$D_{1,4}^{INT}$	$D_{1,5}^{INT}$
PRBs	0.47	0.98	1.00	1.00	0.29	0.49	0.64	0.81
Buffer Size	0.15	0.32	0.43	0.85	0.29	0.49	0.45	0.78
Throughput	0.13	0.29	0.36	0.82	0.13	0.22	0.21	0.41
Severity σ^K	0.14	0.30	0.40	0.84	0.21	0.35	0.33	0.59

how the PRBs are internally allocated to users of each slice) policies to satisfy slice-specific intents. Specifically, they all aim at maximizing eMBB throughput and number of mMTC transmitted packets, while minimizing DL buffer size for URLLC traffic (as a proxy of latency). They all target this goal via different action spaces. a_6 controls the scheduling policy only, a_7 controls the slicing policy only, while a_8 controls both the scheduling and the slicing policies. These are referred to as Sched 0.5, Slicing 0.5, Sched & Slicing 0.5 in [27], respectively. These xApps embed agents trained using Proximal Policy Optimization (PPO), a state-of-the-art Reinforcement Learning (RL) architecture [28], and are deployed inside the Near-RT RIC. They receive real-time KPMs via the E2 interface, make decisions based on network conditions such as downlink throughput, buffer occupancy, and the number of transmitted packets, and continuously adapt their control policies based on real-time feedback from the RAN. It is noted that the model-free architecture and trial-and-error approach of the PPO algorithm are an ideal fit for enhancing the resource allocation process in stochastic environments, such as wireless channels. Ultimately, our goal is to demonstrate that xApps with similar intents, even when controlling different parameters, are prone to generating minimal conflicts.

9.2 Experimental Results

In our experiments, we consider both K-S and INT distances (shown in Tab. 1). The conflict analysis and report generation are performed by the Conflict Detection and Conflict Evaluation modules. In our prototype, both modules are implemented in MATLAB. In the following, distances between control parameters refer to direct conflicts, while distances between KPMs refer to KPM conflicts. In our analysis, the set of parameters and KPMs considered consists of PRBs, Scheduling Policy, Buffer Size, and Throughput, since these show correlation with all the other KPMs that

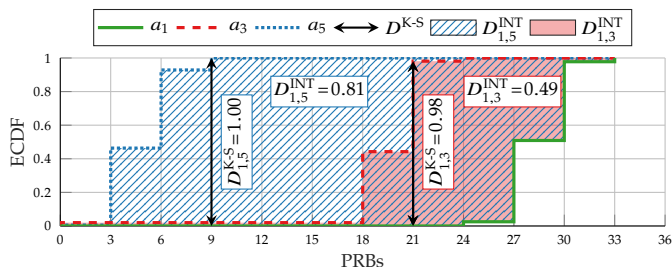


Fig. 13: ECDFs of the number of PRBs assigned to the eMBB slice of xApps a_1 , a_3 , and a_5 and corresponding K-S and INT distances.

have been collected to assess the network performance. In the following section, results are shown for slices eMBB and URLLC only, excluding slice mMTC because slice URLLC and mMTC have similar characteristics and show similar results. Moreover, although we only consider downlink KPMs, PACIFISTA is agnostic to the physical meaning of KPMs and only focuses on how actions taken by any O-RAN application impact the value of such KPMs.

9.2.1 Relevance of Different Distance Functions

We first illustrate how the K-S distance is a good indicator for detecting conflicts, while the INT distance brings more granular insights on conflict severity. This is shown in Tab. 2, where we compare K-S and INT distances taking xApp a_1 as reference. In general, we notice that K-S distances are larger than INT. This is better illustrated in Fig. 13, where we notice that the K-S distances between a_1 and a_3 , and a_1 and a_5 are both close to 1, thus showing the existence of direct conflict. However, the INT distances in the two cases are 0.49 and 0.81, respectively. This shows that although there is direct conflict in both cases, this is less severe in the a_1 - a_3 case than in the a_1 - a_5 case as a_1 and a_3 compute similar slicing policies. The last row in Tab. 2 also shows conflict severity measured using an average combining function $H(\cdot)$ with \mathcal{K}^* containing both downlink throughput and buffer size. As expected, conflict severity increases with KPM distances which, in this case, are averaged via $H(\cdot)$. Severity indexes calculated using INT distances for all stochastic xApps are also reported in Tab. 3 and 4 for eMBB and URLLC slices, respectively.

We notice that conflicts impact largely the eMBB slice, where xApps that allocate less PRBs to eMBB (e.g., a_4 , a_5) severely degrade throughput (i.e., target KPM for eMBB). Instead, since URLLC requests less traffic, we notice that conflict severity is very small and close to 0 in general, i.e., URLLC is minimally affected by KPM conflicts caused by xApps with high direct conflicts as the buffer is emptied even with the few PRBs allocated by a_1 to URLLC.

9.2.2 DRL-Based xApps

In the first experiment, we consider xApps a_6 - a_8 which use DRL agents with diverse action spaces to improve slice-specific KPMs (Section 9.1.2). Due to space limitations, we only present conflict analysis for eMBB and URLLC slices. We report downlink throughput values for the former, and downlink buffer size for the latter. Tab. 5 shows the K-S and INT distances for numerical parameters (i.e., slicing policies) and KPMs, and χ distance for scheduling policies, as well as the impact of conflicts on relevant KPMs. Recall that a_8 controls both slicing and scheduling policies, while

TABLE 3: Severity indexes σ^K using INT distance for eMBB. TABLE 4: Severity indexes σ^K using INT distance for URLLC.

	a_1	a_2	a_3	a_4	a_5
a_1	.00	.21	.35	.33	.59
a_2	.21	.00	.28	.26	.55
a_3	.35	.28	.00	.19	.48
a_4	.33	.26	.19	.00	.00
a_5	.59	.55	.48	.00	.00

	a_1	a_2	a_3	a_4	a_5
a_1	.0000	.0101	.0121	.0123	.0134
a_2	.0101	.0000	.0066	.0071	.0088
a_3	.0121	.0066	.0000	.0047	.0064
a_4	.0123	.0071	.0047	.0000	.0000
a_5	.0134	.0088	.0064	.0000	.0000

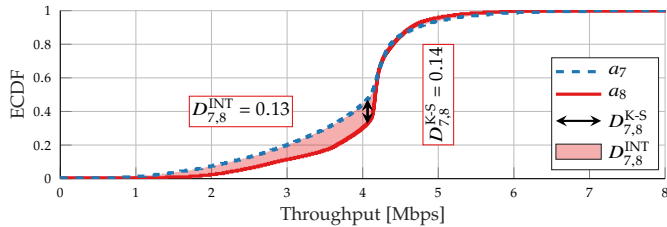


Fig. 14: ECDFs of throughput of the eMBB slice for xApps a_7 and a_8 , highlighting the expected KPM conflict for that control parameter.

a_6 and a_7 respectively control scheduling and slicing only. Therefore, there is no direct conflict on scheduling between a_8 and a_7 , and no direct conflict on slicing between a_8 and a_6 . Since a_7 and a_8 both control slicing policies, they generate a direct conflict with K-S and INT distance equal to 0.11 and 0.23, respectively. The same holds for a_6 and a_8 which produce a direct conflict with respect to scheduling with a χ distance of 0.61, suggesting that the two xApps select different scheduling policies. In general, conflicts have low values due to the shared goal. However, we notice that controlling slicing policies (i.e., a_7 and a_8) results in lower KPM conflicts for both throughput and buffer size (i.e., the largest distance in this case is $D_{8,7}^{K-S} = 0.14$), suggesting that controlling slicing policies under a shared goal makes it possible to achieve higher performance than scheduling control alone [27], which allows the xApps to better satisfy the shared intent and produce less conflicts. We also notice that the larger action space (i.e., scheduling and slicing) allows a_8 to improve performance. For example, Fig. 14 shows how a_8 delivers higher eMBB throughput than a_7 .

9.2.3 Stochastic xApps

To highlight differences between xApps with conflicting intents, we consider xApps a_1 - a_5 from Section 9.1.1. We report allocated PRBs for all slices, while only downlink throughput and buffer size are shown for eMBB and URLLC, respectively. Tab. 6 reports conflict values for both eMBB and URLLC, as well as performance variation when two xApps with different severity indexes (i.e., a_1 , a_2 and a_5) execute at the same time.

Since xApps a_1 and a_2 have similar ECDFs (see Fig. 12), Tab. 6 shows low INT distance for eMBB and URLLC slices with respect to both direct (i.e., PRB number) and KPM (i.e., throughput and buffer size) conflicts. On the

TABLE 5: Direct and KPM conflict analysis taking a_8 as the reference xApp.

Slice	Variable	a_8 - a_6			a_8 - a_7		
		$D_{8,6}^{K-S}$	$D_{8,6}^{INT}$	$D_{8,6}^{\chi}$	$D_{8,7}^{K-S}$	$D_{8,7}^{INT}$	$D_{8,7}^{\chi}$
eMBB	PRBs	0	0	-	0.11	0.23	-
eMBB	Scheduling	-	-	0.61	-	-	0
eMBB	Throughput	0.46	0.27	-	0.14	0.13	-
URLLC	PRBs	0	0	-	0.10	0.16	-
URLLC	Scheduling	-	-	0.19	-	-	0
URLLC	Buffer Size	0.06	0.01	-	0.04	0.01	-

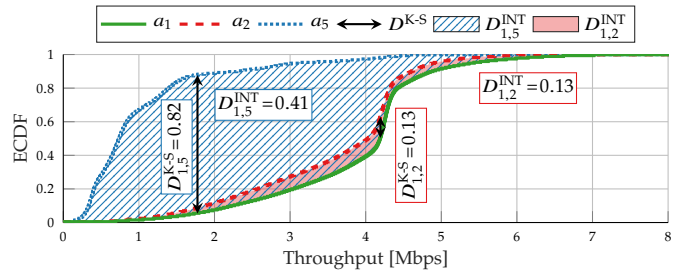


Fig. 15: ECDFs of throughput of the eMBB slice for xApps a_1 , a_2 , and a_5 , highlighting the expected KPM conflict for that control parameter.

contrary, a_1 and a_5 show high INT and K-S distances with respect to PRB number and throughput (i.e., high direct and KPM conflicts). However, a_1 and a_5 have low KPM conflict with respect to buffer size for URLLC, which has an INT distance of 0.01. These differences are also illustrated in Fig. 15, where we focus on conflicts related to throughput of the eMBB slice. This demonstrates the importance of individually analyzing direct and KPM conflicts, as large direct conflicts (i.e., INT distance between a_1 and a_5 with respect to PRB number for URLLC slice) can result in low KPM conflicts (i.e., URLLC buffer size in the same case) due, for example, to traffic demand.

9.2.4 Importance of Mitigating Conflicts and Impact on KPMs

Mitigating conflicts is essential to avoid conflicting control decisions causing performance degradation and unstable behavior, as previously shown in Fig. 1, where a_1 and a_5 were used as the xApp ES and TM, respectively.

PACIFISTA evaluates how two applications generate control policies that conflict on action values (e.g., how far away the two actions are) and KPMs (e.g., how to actions impact the KPMs). Conflicts are differentiated into three categories to identify which conflicts only cause different actions (but same KPMs), and which cause different actions with different KPM values. Therefore, the system provides you with statistical information on how two applications will impact system performance, and then the operator can determine a threshold to identify what is a severe conflict that needs to be mitigated/prevented, and what is a conflict that can be tolerated.

In Tab. 6, we associate K-S and INT distances with performance variation. We consider a_1 as the baseline xApp and evaluate distance and KPM values if compared to a_2 and a_5 . As shown in Fig. 12 and summarized in Tab. 6, a_1

TABLE 6: Direct and KPM conflict analysis taking a_1 as the reference xApp.

Slice	Variable	a_1 - a_2			a_1 - a_5		
		$D_{1,2}^{K-S}$	$D_{1,2}^{INT}$	Variation [%]	$D_{1,5}^{K-S}$	$D_{1,5}^{INT}$	Variation [%]
eMBB	PRBs	0.47	0.29	-8.64	1.00	0.81	-25.93
eMBB	Throughput	0.13	0.13	-16.42	0.82	0.41	-31.80
URLLC	PRBs	0.48	0.28	51.37	1.00	0.65	94.47
URLLC	Buffer Size	0.07	0.01	-84.21	0.14	0.01	-76.53

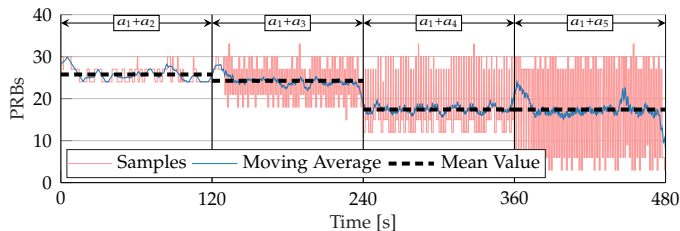


Fig. 16: Impact of conflicts on the stability of the network for the eMBB slice.

and a_2 have a low direct and KPM conflict with K-S and INT with respect to PRB number allocated to eMBB of 0.29 and 0.13, respectively. If compared to a_1 , Tab. 6 shows that a_2 allocates $\approx 8.6\%$ less PRBs to eMBB with an INT severity index $\sigma_{1,2}^K = 0.21$ (reported in Tab. 3), which results in a $\approx 16.4\%$ reduction in throughput. On the contrary, a_5 has a K-S and INT distance of respectively 0.81 and 0.41, and an INT severity index $\sigma_{1,5}^K = 0.59$. This highlights a more severe conflict that is demonstrated by the fact that a_5 allocates $\approx 26\%$ less PRBs to eMBB (i.e., $\approx 2.8\times$ less than a_2), which results in a 31.8% reduction in throughput (i.e., $1.92\times$ higher than a_2).

However, Tab. 4 shows that URLLC still enjoys low buffer size even in the case of xApps with high direct conflict (i.e., a_1 and a_5), and the severity of KPM conflicts σ^K never exceeds 0.02. For example, Tab. 6 shows that a_2 allocates to URLLC 51% more PRBs than a_1 , which results in a 84% reduction in buffer size. That is, what the eMBB slice perceives as a conflict, actually benefits URLLC, demonstrating the need for a fine-grained conflict analysis framework such as PACIFISTA to evaluate how conflicts impact intents and target KPMs.

Stability is another drawback caused by conflicts. In Fig. 16, we report the PRB allocation for the eMBB slice resulting from an 8-minute coexistence experiment in which we keep xApp a_1 always active, and iteratively activate a stochastic xApp every 2 minutes. We notice that the greater the direct conflict between the xApps (reported in Tab. 2), the larger the oscillations in the number of PRBs allocated to the eMBB slice. This is also confirmed by the computation of three statistical metrics: namely the Coefficient of Variation (COV), the Standard Deviation (SD), and the Root Mean Square of Successive Differences (RMSSD). All three metrics considered represent a measure of the oscillation amplitude of the variable considered (assigned PRBs in this case), and they all grow as the conflict increases, as shown in Fig. 17. This might cause unstable behavior due to frequent updates of control parameters using conflicting policies that prevent a coordinated and orchestrated effort in satisfying intents.

Finally, in Tab. 7, we provide two examples for different values of the conflict tolerance δ^{TOL} with respect to the eMBB slice and its conflict severity indexes from Tab. 3. Specifically, we show how conflict tolerance specified by operators impacts the number of xApps that can coexist in the Near-RT RIC. We show the xApps that can be instantiated for a certain value of δ^{TOL} in green, and those that cannot coexist due to high conflicts in red. We notice that low tolerance (i.e., $\delta^{\text{TOL}} = 0.25$) heavily limits the number of coexisting xApps, while a larger tolerance

TABLE 7: Coexistence under tolerance $\delta^{\text{TOL}} = 0.25$ (left) and $\delta^{\text{TOL}} = 0.5$ (right).

	a_1	a_2	a_3	a_4	a_5		a_1	a_2	a_3	a_4	a_5
a_1	0.00	0.21	0.35	0.33	0.59	a_1	0.00	0.21	0.35	0.33	0.59
a_2	0.21	0.00	0.28	0.26	0.55	a_2	0.21	0.00	0.28	0.26	0.55
a_3	0.35	0.28	0.00	0.19	0.48	a_3	0.35	0.28	0.00	0.19	0.48
a_4	0.33	0.26	0.19	0.00	0.00	a_4	0.33	0.26	0.19	0.00	0.00
a_5	0.59	0.55	0.48	0.00	0.00	a_5	0.59	0.55	0.48	0.00	0.00

threshold (i.e., $\delta^{\text{TOL}} = 0.5$) leads to a more diverse xApp deployment. Combining these results with the performance degradation reported in Tab. 6, we show that PACIFISTA can effectively help operators in preventing deployment of applications that would impact KPMs above a certain tolerance threshold. For example, setting $\delta^{\text{TOL}} = 0.25$ limits coexistence of xApp a_1 to a_2 only (maximum decrease of throughput for the eMBB slice of -16.42%) and prevents, for instance, deployment of xApp a_5 which would reduce the same KPM by approximately 32%.

10 CONCLUSIONS

In this paper, we proposed PACIFISTA, a framework to detect, characterize, and mitigate conflicts in the O-RAN ecosystem. PACIFISTA leverages statistical information on O-RAN applications and a set of hierarchical graphs to determine the likelihood of conflict emergence and the corresponding severity. We derived a formal, data-driven model that PACIFISTA uses to capture the impact of conflicts on control parameters and target KPMs, thus providing useful insights on how conflicts affect the network performance and the operator's intents. We also proposed a tunable conflict mitigation strategy that uses PACIFISTA statistical analysis to determine which O-RAN applications can coexist, and which should not be deployed to prevent performance degradation. We prototyped PACIFISTA on a real-world O-RAN testbed and carried out an experimental campaign that demonstrated PACIFISTA's effectiveness in characterizing conflicts and providing insights for informed deployment decisions.

Future work will focus on three aspects: (i) extracting a model to capture the relationship between conflict severity and the performance degradation of the RAN to predict performance degradation before applications are deployed; (ii) how the impact of asynchronous actions generated by different applications affects conflicts severity; and (iii) what strategies can be developed and implemented by the network operator to adaptively express thresholds for the mitigation phase.

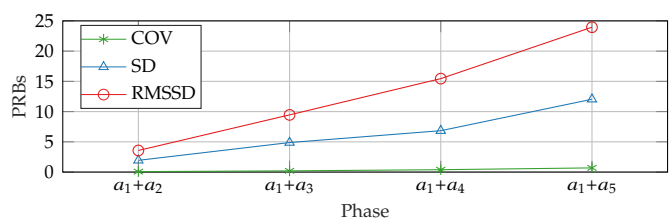


Fig. 17: COV, SD, and RMSSD for the eMBB slice.

REFERENCES

- [1] M. Polese, L. Bonati, S. D'Oro, S. Basagni, and T. Melodia, "Understanding O-RAN: Architecture, Interfaces, Algorithms, Security, and Research Challenges," *IEEE Communications Surveys & Tutorials*, vol. 25, no. 2, pp. 1376–1411, January 2023.
- [2] O-RAN Working Group 1, "O-RAN Use Cases Detailed Specification 6.0," O-RAN.WG1.Use-Cases-Detailed-Specification-v06.00 Technical Specification, July 2021.
- [3] T. Pamuklu, S. Mollahasani, and M. Erol-Kantarci, "Energy-Efficient and Delay-Guaranteed Joint Resource Allocation and DU Selection in O-RAN," in *IEEE 4th 5G World Forum (5GWF)*, 2021, pp. 99–104.
- [4] S. D'Oro, L. Bonati, M. Polese, and T. Melodia, "OrchestRAN: Network Automation Through Orchestrated Intelligence in the Open RAN," in *Proceedings of IEEE INFOCOM*, 2022.
- [5] C. Adamczyk, "Challenges for Conflict Mitigation in O-RAN's RAN Intelligent Controllers," in *Proceedings of IEEE SoftCOM*, 2023.
- [6] C. Adamczyk and A. Kliks, "Conflict Mitigation Framework and Conflict Detection in O-RAN Near-RT RIC," *IEEE Communications Magazine*, 2023.
- [7] A. Wadud, F. Golpayegani, and N. Afraz, "QACM: QoS-Aware xApp Conflict Mitigation in Open RAN," *arXiv preprint arXiv:2405.07324*, 2024.
- [8] P. E. Iturria-Rivera, H. Zhang, H. Zhou, S. Mollahasani, and M. Erol-Kantarci, "Multi-agent team learning in virtualized open radio access networks (O-RAN)," *Sensors*, vol. 22, no. 14, p. 5375, 2022.
- [9] H. Zhang, H. Zhou, and M. Erol-Kantarci, "Team learning-based resource allocation for open radio access network (O-RAN)," in *ICC 2022-IEEE International Conference on Communications*. IEEE, 2022, pp. 4938–4943.
- [10] S. D'Oro, M. Polese, L. Bonati, H. Cheng, and T. Melodia, "dApps: Distributed applications for real-time inference and control in O-RAN," *IEEE Communications Magazine*, vol. 60, no. 11, pp. 52–58, 2022.
- [11] L. Bonati, M. Polese, S. D'Oro, S. Basagni, and T. Melodia, "OpenRAN Gym: AI/ML Development, Data Collection, and Testing for O-RAN on PAWR Platforms," *Computer Networks*, vol. 220, 2023.
- [12] E. Lupu and M. Sloman, "Conflicts in Policy-based Distributed Systems Management," *IEEE Transactions on Software Engineering*, vol. 25, no. 6, November 1999.
- [13] C. Tessier, L. Chaudron, and H.-J. Müller, *Conflicting agents: conflict management in multi-agent systems*. Springer Science & Business Media, 2005, vol. 1.
- [14] F. Cuppens, N. Cuppens-Boulahia, and M. B. Ghorbel, "High level conflict management strategies in advanced access control models," *Electronic Notes in Theoretical Computer Science*, vol. 186, pp. 3–26, 2007.
- [15] J. Lee, "Conflict resolution in multi-agent based Intelligent Environments," *Building and Environment*, vol. 45, no. 3, pp. 574–585, 2010.
- [16] O-RAN Working Group 1, "O-RAN Architecture Description 11.00," O-RAN.WG1.O-RAN-Architecture-Description-v11.00 Technical Specification, February 2024.
- [17] W. Li, J. Zhang, and Y. Zhao, "Conflict graph embedding for wireless network optimization," in *IEEE Conference on Computer Communications*. IEEE, 2017, pp. 1–9.
- [18] L.-j. Chen, T. Sun, and M. Gerla, "Modeling Channel Conflict Probabilities between IEEE 802.15 based Wireless Personal Area Networks," in *Proceedings of IEEE International Conference on Communications*, 2006.
- [19] N. Yungaiçela-Naula, V. Sharma, and S. Scott-Hayward, "Misconfiguration in O-RAN: Analysis of the impact of AI/ML," *arXiv preprint arXiv:2403.01180*, 2024.
- [20] A. Zolghadr, J. F. Santos, L. A. DaSilva, and J. Kibilda, "Learning and Reconstructing Conflicts in O-RAN: A Graph Neural Network Approach," *arXiv preprint arXiv:2412.14119*, 2024.
- [21] O-RAN Working Group 3, "Conflict Mitigation," O-RAN.WG3.TR.ConMit-R004-v01.00 Technical Specification, October 2024.
- [22] A. Nichols, "Causal inference with observational data," *The Stata Journal*, vol. 7, no. 4, pp. 507–541, 2007.
- [23] D. Villa, M. Tehrani-Moayyed, C. P. Robinson, L. Bonati, P. Johari, M. Polese, and T. Melodia, "Colosseum as a Digital Twin: Bridging Real-World Experimentation and Wireless Network Emulation," *IEEE Transactions on Mobile Computing*, pp. 1–17, January 2024.
- [24] Unwired Labs. (2024, November) OpenCelliD. <https://opencellid.org>. Accessed April 2024.
- [25] A. Hazra and N. Gogtay, "Biostatistics series module 4: comparing groups—categorical variables," *Indian journal of dermatology*, vol. 61, no. 4, pp. 385–392, 2016.
- [26] U.S. Naval Research Laboratory, "MGEN Traffic Emulator," February 2024, accessed April 2024. [Online]. Available: <https://www.nrl.navy.mil/Our-Work/Areas-of-Research/Information-Technology/NCS/MGEN>
- [27] M. Tsampazi, S. D'Oro, M. Polese, L. Bonati, G. Poitau, M. Healy, and T. Melodia, "A Comparative Analysis of Deep Reinforcement Learning-based xApps in O-RAN," in *Proceedings of IEEE GLOBECOM*, Kuala Lumpur, Malaysia, December 2023.
- [28] W. Chen, Y. Chen, Y. Wang, and R. Liu, "Static Standing Balance With Musculoskeletal Models Using PPO With Reward Shaping," *Procedia Computer Science*, vol. 226, pp. 78–84, 2023.

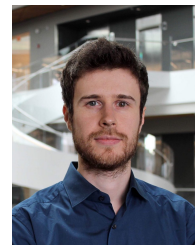


Pietro Brach del Prever is a Ph.D. Candidate at the Institute for the Wireless Internet of Things at Northeastern University. He graduated at Politecnico di Torino in Mechatronic Engineering in 2022, and in Mechanical Engineering in 2020. He visited the University of Porto in 2019 and the Technion Israel Institute of Technology in 2021 as an exchange student. He also graduated from Alta Scuola Politecnica, a joint honor program of Politecnico di Torino and Politecnico di Milano for the top 1% students of both universities. His

research interests include wireless networks optimization, and intrabody communication.



Salvatore D'Oro is a Research Associate Professor at Northeastern University. He received his Ph.D. degree from the University of Catania and is an area editor of Elsevier Computer Communications journal. He serves on the TPC of IEEE INFOCOM, IEEE CCNC & ICC and IFIP Networking. He is one of the contributors to OpenRAN Gym, the first open-source research platform for AI/ML applications in the Open RAN. His research interests include optimization, AI & network slicing for NextG Open RANs.



Leonardo Bonati is an Associate Research Scientist at the Institute for the Wireless Internet of Things, Northeastern University. He received a Ph.D. degree in Computer Engineering from Northeastern University in 2022. His research focuses on softwareized approaches for the Open RAN of next generation of cellular networks, on O-RAN-managed networks, and on network automation and orchestration. He served as guest editor of the special issue of Elsevier's Computer Networks journal on Advances in Experimental

Wireless Platforms and Systems.



Michele Polese is a Research Assistant Professor at Northeastern University. He received his Ph.D. from the University of Padova, while his research is funded by the US NSF, OUDS, and NTIA. He holds several best paper awards and the '22 Mario Gerla Award for Research in Computer Science. He is a TPC co-chair for WNS3 '22, an Associate Technical Editor for the IEEE Communications Magazine, and a Guest Editor in JSAC's Special Issue on Open RAN.



Maria Tsampazi received her MEng Degree in ECE from National Technical University of Athens, Greece in '21. She is a Ph.D. Candidate in Electrical Engineering at the Institute for the Wireless Internet of Things, NEU. Her research focuses on NextG networks and intelligent resource allocation in Open RAN. She has received academic awards sponsored by the US NSF, IEEE ComSoc & NEU, and is a National Spectrum Consortium Woman in Spectrum scholarship recipient. Maria has collaborated with government and industry organizations such as the US DoT and Dell Technologies.



Heiko Lehmann Heiko Lehmann is Tribe Lead for Cybersecurity and Digital Twin at in Deutsche Telekom's Group Technology Division. He is affiliated with T-Labs. Trained a physicist, he received a Ph.D. in Theoretical Physics from Humboldt University Berlin in 1992. Following post-doctoral academic work at Oxford University and the German National Society for Mathematics and Informatics, he joined the telematics subsidiary of Volkswagen Group in 1999 where he held the position of Innovation Manager. In 2006,

Lehmann joined T-Labs where he took over responsibility for a portfolio of innovation projects. Recently, he is focusing on Artificial Intelligence and its application to Digital Twins, cybersecurity, self-organization, complex systems and optimization in a wide variety of application areas. Lehmann has published extensively in theoretical physics, informatics, engineering and business topics.



Tommaso Melodia is the William Lincoln Smith Professor at Northeastern University, Director of the Institute for the Wireless Internet of Things and Director of Research for the Platforms for Advanced Wireless Research, a 100M public-private partnership to advance the US wireless ecosystem. He received his Ph.D. from the Georgia Institute of Technology and is a recipient of the NSF CAREER award. He has served as Associate Editor of IEEE Transactions on Wireless Communications, Transactions on Mobile Computing and Elsevier Computer Networks, and as TPC Chair for IEEE INFOCOM '18, General Chair for IEEE SECON '19, ACM Nanocom '19, and WUWnet '14. His research on the experimental evaluation of IoT and wireless networked systems has been funded by the NSF, the Air Force & Army Research Laboratories, the Office of Naval Research, and DARPA. He is an IEEE Fellow and ACM Senior Member.